A new automatic *S*-onset detection technique: Application in local earthquake data

Athanasios Lois[1], Efthimios Sokos[1], Nikolaos Martakis[2], Paraskevas Paraskevopoulos[1], and G-Akis Tselentis[1]

ABSTRACT

Algorithms that deal with the automatic *S*-onset time identification problem are a topic of ongoing research. Modern dense seismic networks used for earthquake location, seismic tomography investigations, source studies, early warning, etc., demand accurate automatic S-wave picking. Most of the techniques that have been proposed up to now are mainly based on the polarization features of the seismic waves. We propose a new time domain method for the automatic determination of the *S*-phase arrival onsets, and present its implementation on local earthquake data. Eigenvalue analysis takes place over small time intervals, and the maximum eigenvalue which is obtained on each step is retained for further processing. In this way, a time series of maximum eigenvalues is formed, which serves as a characteristic function. We obtain a first *S*-phase arrival time estimation by applying the kurtosis criterion on the derived characteristic function. Furthermore, a multiwindow approach combined with an energy-based weighting scheme is also applied, to reduce the algorithm's dependence on the moving window's length and provide a weighted *S*-phase onset. Automatic picks were compared against manual reference picks, resulting in mean residual time of 0.051 s. Moreover, the proposed technique was subjected to a noise robustness test and sustained a good performance. The mean residual time remained lower than 0.1 s, for noise levels between −1 up to 8 dB. The proposed method is easy to implement, because it is almost parameter free and demands low computational resources.

INTRODUCTION

A large number of algorithms have been proposed and used on seismic networks for phase identification. The accurate determination of compressional and transversal seismic waves is important for earthquake location and focal mechanism determination, but is also essential for other applications such as passive seismic tomography investigations (Tselentis et al., 2011b). Regarding the event detection as well as *P*-phase identification, several techniques exist involving energy criteria (Allen, 1978; Baer and Kradolfer, 1987), polarization analysis tests (Montalbetti and Kanasewich, 1970; Vidale, 1986; Magotra et al., 1987; Ruud and Husebye, 1992), fuzzy logic tests (Chu and Mendel, 1994), artificial neural networks (Dai and MacBeth, 1995), higher-order statistics (Saragiotis et al., 2002), wavelet analysis (Anant and Dowla, 1997), etc.

In contrast to *P*-onset time estimation, algorithms that deal with *S*-phase arrival are mainly based on polarization attributes of the seismic signal, and their development is a topic of ongoing research. The identification of phase-arrival times is traditionally done by experienced seismologists, but due to the character of the later-arriving shear waves, even manual S-wave picking is often uncertain and inconsistent. Moreover the *S*-onset time-identification problem can be further complicated due to converted waves, which can be misinterpreted as the direct *S*-onset (Sokos, et al., 2012).

It is well-known that polarization measurements may indicate the arrival of seismic phases, because highly linear particle motion may be associated with body wave arrivals. Using 3C data and linear algebra's fundamentals, Flinn (1965) designed a time-varying nonlinear filter to enhance particle motion which is rectilinear in a particular direction in 3D space. The usefulness of such a detector lies in its ability to separate compressional wave motion from the shear or surface wave motion, when the distance and azimuth to the seismic source is specified.

Montalbetti and Kanasewich (1970) modified the time domain polarization filter originally proposed by Flinn, and used it to increase the signal to noise (S/N) ratio of teleseismic body wave phases. A complex polarization filter was proposed by Vidale (1986) as an extension of the Montalbetti and Kanasewich (1970) scheme, where the imaginary part of the signal is the Hilbert transform of the real part. Another time domain technique based on Flinn's method was proposed by Jurkevics (1988). He extended Flinn's work by including frequency decomposition and the application to arrays of 3C sensors.

Cichowicz (1993) combined the significant characteristics of an S-wave arrival into one characteristic function that consists of a product of different polarization filters such as rectilinearity, directivity, and the ratio between transverse and total energy. Finally, hybrid methods have also been proposed, by Wang and Teng (1997), Saragiotis et al. (1999), Bai and Kennett (2000), Gentili and Michelini (2006), Diehl et al. (2009), Nippres et al. (2010), and Küperkoch et al. (2011), that involve, in addition to polarization analysis, time series analysis techniques, autoregressive prediction, STA/LTA detectors, pattern recognition schemes, artificial neural networks, wavelet analysis, and higher order statistics.

Most of the methods mentioned above are mainly implemented on data from a single 3C receiver. Numerous techniques, however, have been developed and used by the industry, using data recorded by array of receivers. Seismic monitoring with arrays of receivers provides the opportunity to check consistency of signal detection across a seismic network of receivers. For example, Fischer et al. (2007) developed a new method for picking P- and S-waves at a linear receiver array, which employs polarization properties and array consistency of the detected phases. Drew et al. (2005) implemented a method to detect and locate events on data recorded by a vertical array of 3C seismic sensors. According to their method, event detection is continuously updated and applied to a spatial map of the probability of microseismicity occurrence. Finally, one can find the complete state-of-the-art techniques used in the industry regarding surface, near-surface, and downhole monitoring, as nicely summarized and presented by Maxwell et al. (2010) and Duncan and Eisner (2010).

In this paper, we propose an automatic S-wave detector scheme, based on the statistical processing of a specific characteristic function that is obtained by eigenvalue analysis and makes no assumptions about the polarization of P- and S-waves. It is an almost parameter-free algorithm, which is straightforward to implement and demands low computational resources. The proposed method was developed for use, e.g., in local earthquake tomography or seismicity studies. We present its performance on surface seismic data and on single station, because it can be applied on each station separately. Although the problem of the implementation of our technique on arrays of sensors remains to be examined, we believe that it could be addressed, for example, using methods that introduce multichannel sparsity concepts (Vera Rodriguez et al., 2012).

THEORY

In the following section, we describe the basic principles of polarization analysis and explain how the diagonalization of the data covariance matrix relates to the polarization features of a seismic wave. Moreover a brief introduction to higher order statistics (HOS) is presented, and their usefulness on seismic phase automatic picking is also discussed.

Polarization analysis

The problem can be formulated as follows: Given a zero-mean (3×1) data vector $\vec{s}$ in z, n and e space ($z =$ vertical, $n =$ north–south, $e =$ east–west), we need to identify the direction in which projection y exhibits the maximum variance (Magotra et al., 1987). This can be written as a dot product

$$y = \vec{u}^T \vec{s} = [u_1 u_2 u_3] \begin{bmatrix} s_z \\ s_n \\ s_e \end{bmatrix}, \quad (1)$$

where $\vec{u}$ is a unitary vector ($\|\vec{u}\| = 1$), in the direction of the source's azimuth. Vector s is assumed to be zero mean, so for the mean value and variance of y we can write

$$E[y] = E[\vec{u}^T \vec{s}] = 0$$
$$\sigma_y^2 = E[y^2] = \vec{u}^T C_s \vec{u}, \quad (2)$$

where $E[.]$ denotes the statistical expectation and C_s the covariance matrix of $\vec{s}$

$$C_s = E[\vec{s}\vec{s}^T] = \begin{bmatrix} \sigma_z^2 & \sigma_{zn} & \sigma_{ze} \\ \sigma_{zn} & \sigma_n^2 & \sigma_{ne} \\ \sigma_{ze} & \sigma_{ne} & \sigma_e^2 \end{bmatrix}, \quad (3)$$

where

$$\sigma_z^2 = E[z^2], \quad \sigma_n^2 = E[n^2], \quad \sigma_e^2 = E[e^2]$$

and

$$\sigma_{zn} = E[zn], \quad \sigma_{ne} = E[ne], \quad \sigma_{ze} = E[ze].$$

The projection's variance σ_y^2 can be maximized, using Lagrange multipliers, given the constraint $\|\vec{u}\| = 1$. The above procedure is equal to the maximization of the following expression

$$\Phi(\vec{u}; \lambda) = \sigma_y^2 - \lambda(\|\vec{u}\| - 1) = \vec{u}^T C_s \vec{u} - \lambda(\vec{u}^T \vec{u} - 1). \quad (4)$$

By differentiating this expression with respect to $\vec{u}$ and λ, the following partial differential equations are obtained

$$\frac{\partial \Phi}{\partial \lambda} = (\vec{u}^T \vec{u} - 1), \quad (5)$$

and

$$\frac{\partial \Phi}{\partial \vec{u}} = C_s \vec{u} - \lambda \vec{u} = (C_s - \lambda I)\vec{u} = 0. \quad (6)$$

The first equation defines the initial constraint and the second suggests that λ is eigenvalue of the covariance matrix, whereas $\vec{u}$ is the corresponding eigenvector. Moreover, the eigenvectors, obtained by the diagonalization of the covariance matrix, represent an orthonormal base of the 3D space and form an ellipsoid (polarization ellipsoid), that best fits to the data in a least-squares sense. From equation 6, it is clear that the polarization characteristics of a signal

are obtained by solving the eigenvalue problem of the data covariance matrix because, once the principal axes of the polarization ellipsoid are estimated, the particle motion is determined. Using attributes computed from the principal axes, information describing the degree of linear polarization, the directivity of the particle motion, the azimuth of P-wave propagation as well as the apparent incidence angle of rectilinear motion is extracted. For example, according to Jurkevics (1988) if $\lambda_1 > \lambda_2 > \lambda_3$, the rectilinearity is given by the following relation

$$\text{Rect} = 1 - \frac{\lambda_2 + \lambda_3}{2\lambda_1}, \tag{7}$$

which is expected to be close to one for *P* and *S* phases, whereas the planarity of the particle motion is given by

$$\text{Plan} = 1 - \frac{2\lambda_3}{\lambda_1 + \lambda_2}, \tag{8}$$

which is expected to be close to zero for the *P* arrival and close to one for the first S-wave arrival. It is essential to mention, that the above assumption for the S-wave is valid only in the case of an isotropic medium (Eisner et al., 2009). Additionally if $\vec{u}_{ij}$ are the corresponding eigenvectors, with $i = 1, 2, 3$, the three components (vertical, north–south and east–west) and $j = 1, 2, 3$, the three direction cosines then the azimuth of P-wave propagation is given by

$$P_{\text{azimuth}} = \tan^{-1}\left(\frac{\vec{u}_{12}}{\vec{u}_{13}}\right) \tag{9}$$

and the incident angle of rectilinear motion can be obtained by the relation

$$P_{\text{incidence}} = \cos^{-1}(|\vec{u}_{11}|). \tag{10}$$

Higher-order statistics

The mean value, variance, autocorrelation, and power spectrum constitute the first and second-order statistics, respectively, and are extensively used to describe processes that are linear and Gaussian distributed. However, most of the processes in earth sciences deviate from linearity and Gaussianity. Such processes can be studied through higher-order statistics (HOS).

Specifically, let's assume the N-sample, real and zero-mean process $\{X(k)\}$, that is fourth-order stationary. Its second-, third-, and fourth-order moments are defined as (Nikias et al., 1993)

$$R_2(m) = E\{X(k)X(k+m)\}$$
$$R_3(m, n) = E\{X(k)X(k+m)X(k+n)\}$$
$$R_4(m, n, l) = E\{X(k)X(k+m)X(k+n)X(k+l)\}, \tag{11}$$

where $E\{.\}$ denotes the expectation, and for a continuous random variable x is given by

$$E\{x\} = \int_{-\infty}^{\infty} xf(x)\mathrm{d}x, \tag{12}$$

where $f(x)$ is the probability density function of x. Note that $R_2(0)$ equals to the variance $\sigma^2(x)$ of the random variable x. Another set of statistical parameters that can be used, due to their excellent noise-suppressing properties, are cumulants and can be expressed in terms of the moments. The following formulas denote the third- and fourth- order cumulant sequences of $\{X(k)\}$

$$C_3(m, n) = R_3(m, n)$$
$$C_4(m, n, l) = R_4(m, n, l) - 3(R_2(m))^2. \tag{13}$$

For the zero-lag case, that is $m = n = l = 0$, we obtain the skewness $C_3(0, 0)$ and kurtosis $C_4(0, 0, 0)$.

Skewness provides a measure of symmetry of the distribution and is expected to become zero if the distribution is symmetrical. Furthermore, it takes negative values if the distribution contains outliers to the left and positive values in the opposite case. The fourth-order zero-lag cumulant, the kurtosis, provides a measure of heaviness of the tails of the distribution, and takes the value three for Gaussian distributed random variables. Kurtosis values larger than three indicate widening of the distribution, whereas narrowing is indicated for values smaller than three.

HOS parameters were first used in seismic phase automatic identification by Saragiotis et al. (2002) who developed the PAI-S/K algorithm to identify the *P*-onset time of a seismic event. According to this algorithm, skewness and kurtosis, as measures of asymmetry and non-Gaussianity, respectively, are estimated over a moving time window, and they are expected to present maxima in the neighborhood of the *P* arrival, due to the changes of the signal statistics. The location of the maximum slope of these curves is assigned as the final *P*-onset time estimation. In general, when the signal's statistics change the degree of non-Gaussianity is higher than asymmetry (Saragiotis et al., 2002), thus kurtosis takes much higher values than skewness. Because kurtosis is more sensitive on such changes, it provides a better phase detection criterion than skewness. The above statement is confirmed by several automatic *P*-picking experiments on local earthquake data (Lois et al., 2010; Tselentis et al., 2011a) which have shown that the best results were obtained using the kurtosis criterion. Thus, only this HOS parameter is used in the proposed method.

METHODOLOGY

Given an N-length segment of the record, where a seismic event exists and the *P*-arrival time has been estimated, an M-sample time moving window is applied which divides this segment into overlapping parts of the record. On each section, the algebraic eigenvalue problem of the data covariance matrix is solved, that is, the covariance matrix is diagonalized and three eigenvalues $\lambda_1 > \lambda_2 > \lambda_3$ with their corresponding eigenvectors are obtained. Because the same procedure takes place for each time window, three different sequences $\lambda_1(t), \lambda_2(t), \lambda_3(t), t = 1..N$, are formed, giving a measure of the energy in the direction of the three principal axes of the polarization ellipsoid (Figure 1d).

In this work, we consider only the sequence corresponding to the maximum eigenvalue $\lambda_1(t)$, because it is more sensitive to energy changes in the direction of signal's propagation. Moreover, we choose as a characteristic function, the square root of the maximum eigenvalue's curve $f(t) = \sqrt{\lambda_1(t)}$ (Figure 2), rather than $\lambda_1(t)$ itself, due to the property of the square root function to compress

the signal, that is, reduce its dynamical range by increasing its lower values and decreasing its higher values. This enables us to observe small changes in the signal's energy. We also have to mention that, although the logarithm function is usually used to suppress high values and enhance the smaller ones, the characteristic function which is derived by our analysis appears to be smoother and more distinct using the square root function instead of the logarithm. Furthermore, on low S/N the use of logarithm weakens the performance of the algorithm, because it provides residual times almost two times larger than the ones obtained by the proposed technique.

The next step is to evaluate the square root values of kurtosis $\sqrt{\mathrm{kur}(f(t))}$ on the part of the characteristic function $f(t)$, corresponding to the time section starting a few samples after the P-arrival t_P, up to the end of the seismic event t_{coda}, which have been estimated by the detection algorithm. The selection of the specific segment of the record is necessary, for avoiding erroneous picks such as the P-arrival, and for providing also a time window where the S-wave exists. Specifically, on this part of the record, kurtosis is evaluated over a sliding M-sample overlapping moving window, using the estimator

$$\mathrm{kur}(f(t)) = \frac{\sum_{t=1}^{M}(f(t) - \hat{m}_f)^4}{(M-1)\hat{\sigma}_f^4}, \qquad (14)$$

where $\hat{m}_f$ and $\hat{\sigma}_f$ are the estimators of the mean value and standard deviation of $f(t)$, respectively, and M is the length of the moving window.

During the S-wave arrival (Figure 3b), the values of kurtosis of $f(t)$ present a steep increment due to the change of the signal statistics (Figure 3d). Furthermore, with close inspection we can observe that the S-onset time coincides with the point where the values of the sequence begin to increase and not with the maximum value of the curve. This can be explained by the fact that the maximum value is reached only when a sufficient fraction of the time window contains the S-wave, which is beyond the S-arrival. Thus, the maximum slope is needed to be assessed through signal's first difference (Figure 3e). The location of the initial S-onset time estimation is given by the maximum value of the first difference of the sequence $K(t) = \sqrt{\mathrm{kur}(f(t))}$, that is

$$S_{\mathrm{on}} = \max_t(\Delta K(t)), \qquad t \in [t_P, t_{\mathrm{coda}}], \qquad (15)$$

where Δ refers to the first difference operator $\Delta K(t) = K(t) - K(t-1)$. An important issue that needs to be addressed is the choice of the sliding window's length, which is the only parameter of the algorithm that has to be set. A too-short window results in early picks, because the algorithm becomes too sensitive to small changes. On the other hand, by setting long time window duration, it is possible to obtain picks that are beyond the real S-wave arrival.

To overcome the two aforementioned cases of false alarm, a multiwindow approach accompanied with a weighting scenario is proposed, as a correction procedure. For each S-arrival time estimation, an automatically evaluated uncertainty index is introduced for evaluating the probability of a false alarm. This quality measure, similar to S/N, is based on an energy ratio estimated on the two horizontal
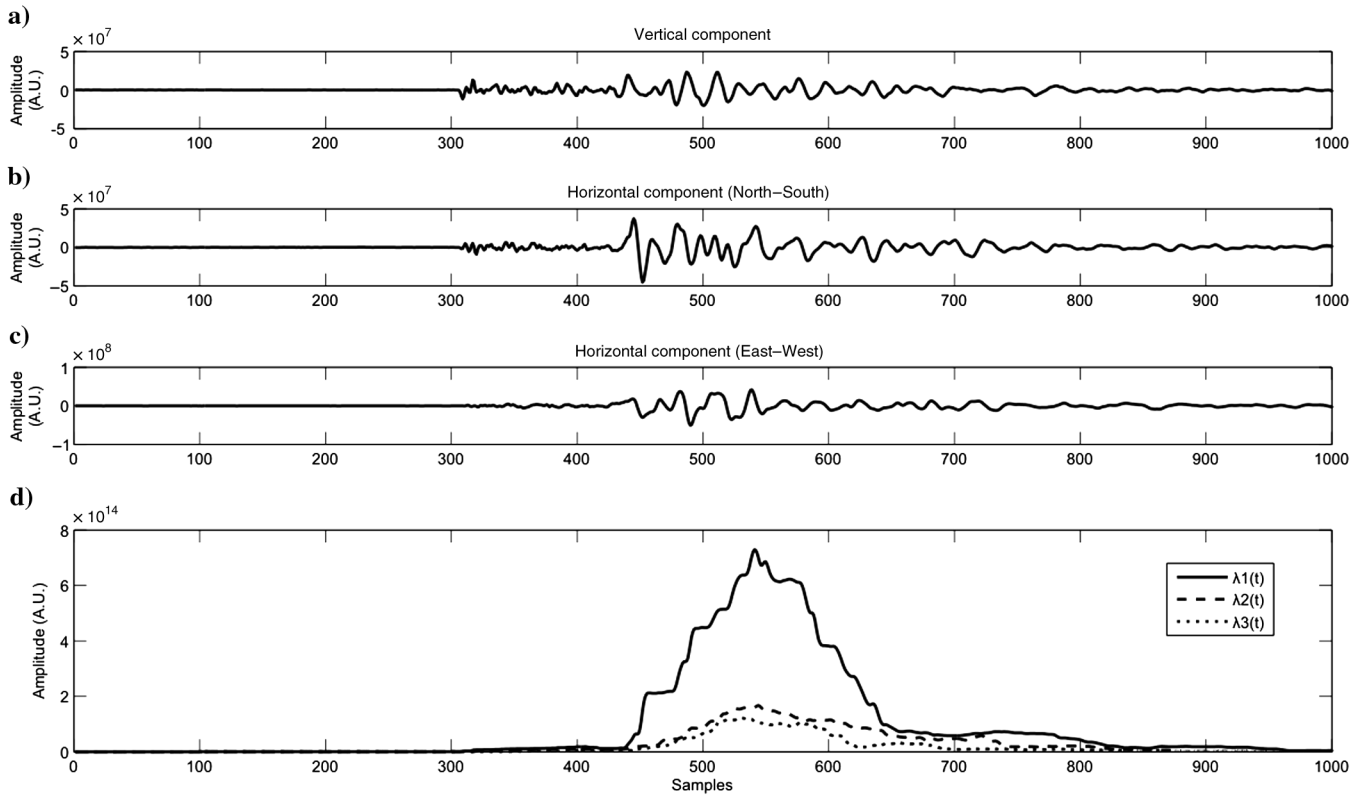

Figure 1. Example of the vertical (a), north–south (b), and east–west (c), components of a seismic signal, and (d) the corresponding sequences obtained by the eigenvalues.
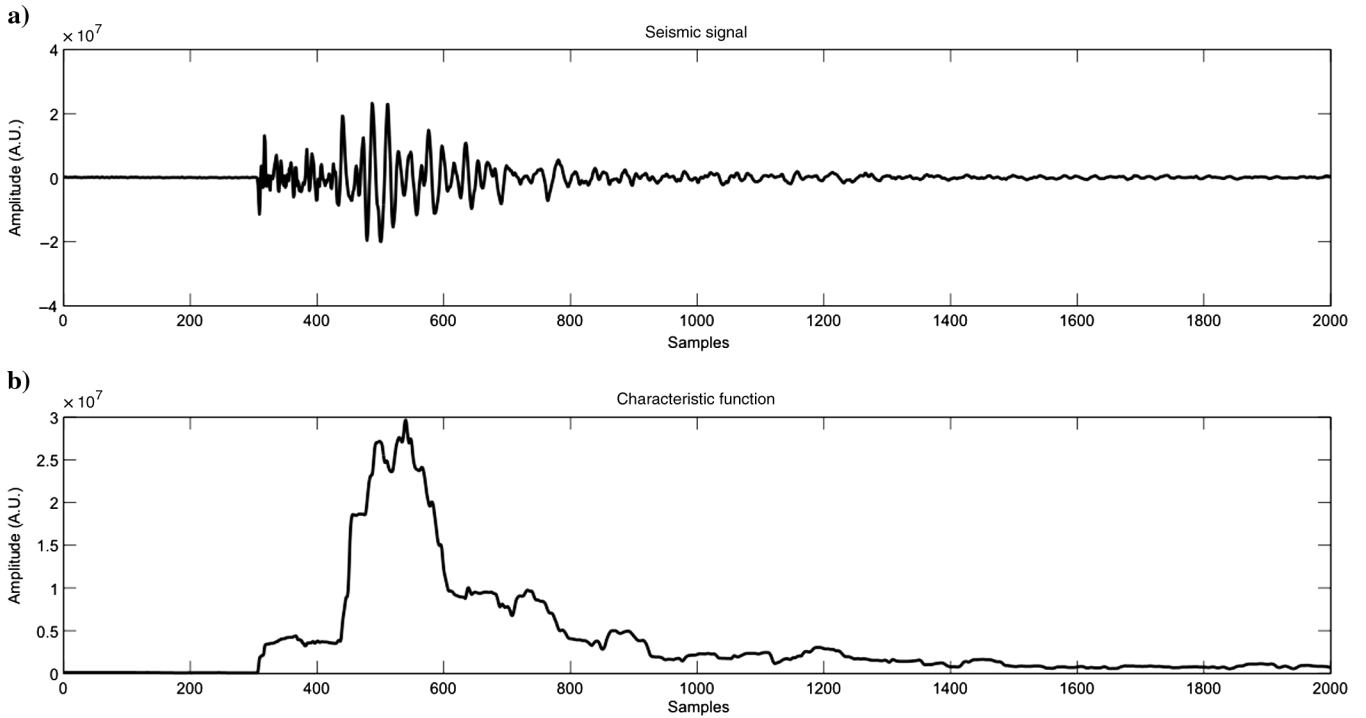
a)

b)

Figure 2. Example of a seismic signal (a) and the characteristic function based on the maximum eigenvalue (b).
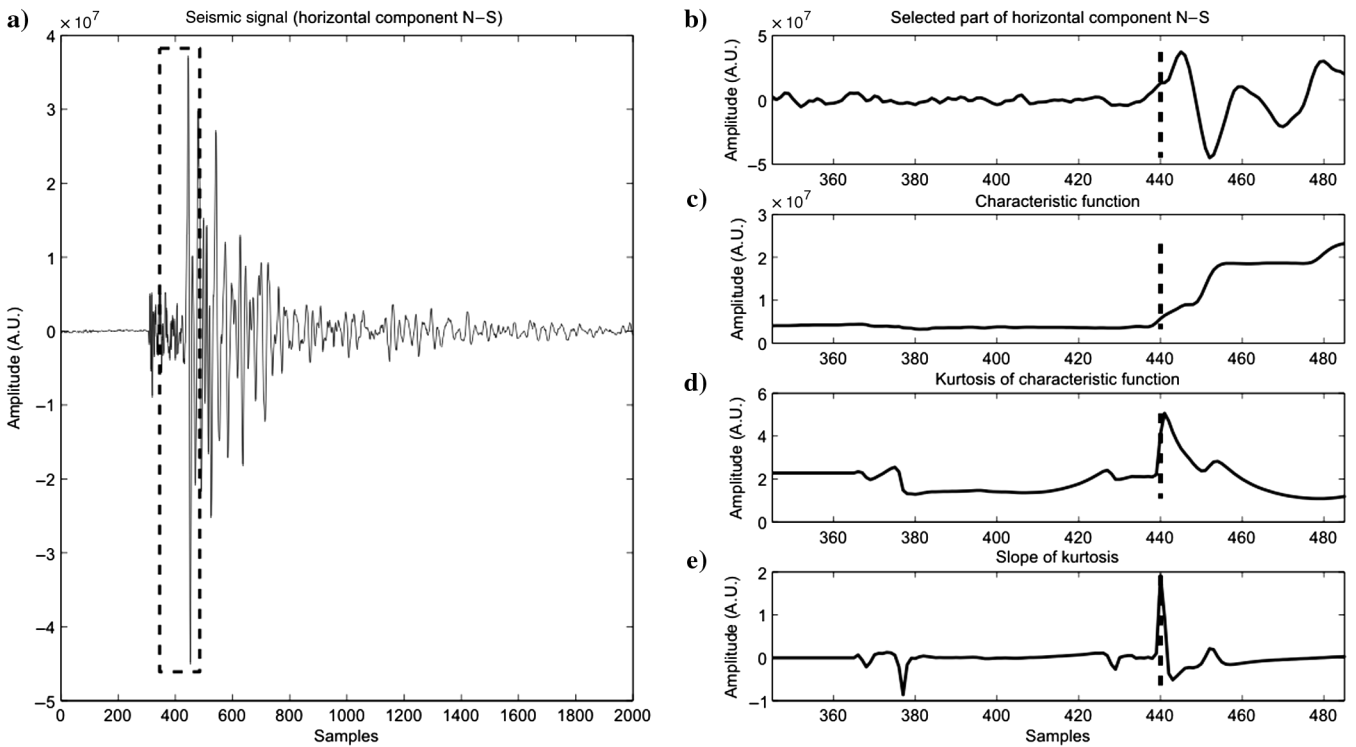
a)

b)

c)

d)

e)

Figure 3. Example of the algorithm's performance on a good-quality signal, using a 0.6 s moving window. Seismic signal (a), the selected part of the signal as indicated in (a), by a dashed rectangle (b), the characteristic function (c), kurtosis of the characteristic function (d), and the slope of kurtosis evaluated through its first derivative (e). The dashed line corresponds to the automatic pick as estimated by the algorithm.

components, into a predefined time section $[S_{on} - t, S_{on} + t]$ and is given in dB by the relation

$$q = 20\log_{10}\left(\frac{\sigma_{S_{on}}}{\sigma_{P\text{coda}}}\right), \qquad (16)$$

where S_{on} is the automatically estimated S-arrival time, $\sigma_{S_{on}}$ and $\sigma_{P\text{coda}}$ are the standard deviations evaluated on the time windows $[S_{on}, S_{on} + t]$ and $[S_{on} - t, S_{on}]$, respectively, and t is time in seconds that is selected empirically according to the S-P difference of the examined seismic events. For example, during the arrival of the S-wave, the energy of the signal usually increases, thus if the automatic pick is close to the real one, positive values of q are expected. On the other hand, an early pick is expected to have q-values close to zero, while a negative q indicates a false pick, because there is no probability of existing P-coda waves with higher energy than the S-waves. Nevertheless, it has to be mentioned that a q value close to zero corresponding to a low-quality pick, does not necessarily indicate a false pick, but shows a case where the seismic signal's energy during the S-wave arrival does not change significantly and careful human analyst's inspection is needed.

The algorithm is applied on the seismic data using windows with various lengths, providing a set $\{S_{on}^i\}_{i=1...w}$ of S-arrival times with the corresponding qs which are used as weights. The final S-onset time estimation is given by the weighted mean of the set $\{S_{on}^i\}_{i=1...w}$

$$S_{\text{final}} = \frac{\sum_{i=1}^{w} S_{on}^i q_i}{\sum_{i=1}^{w} q_i}, \qquad (17)$$

where S_{on}^i are the estimations obtained by the algorithm and form the set of solutions, q_i are the corresponding weights, whereas the index $i = 1, 2, ..w$ indicates the number of the different time windows used. Applying this weighting scheme, possible outliers (false picks) are eliminated by the algorithm, because they obtain weights with values close to zero. Following the same approach, the overall quality q_{final} of the final estimation S_{final} is evaluated and four classes of uncertainty A, B, C, and D are defined as follows

$$\text{Uncertainty class} = \begin{cases} A, & \text{if } q_{\text{final}} > 10 \\ B, & \text{if } 6 < q_{\text{final}} < 10 \\ C, & \text{if } 2 < q_{\text{final}} < 6 \\ D, & \text{if } q_{\text{final}} < 2 \end{cases}. \times \quad (18)$$

Class A corresponds to high-quality picks, B and C to moderate, and D shows poor-quality picks corresponding to high probability of false alarm. A pick which is assigned to a negative quality index is indicated as a false pick as previously mentioned. Although the four uncertainty classes are defined empirically according to our experience on this kind of data, equation 18 could be a useful tool for analysts, because it could provide recommendation regarding necessity of manual reprocessing.

DATA

After the occurrence of an M_w 4.7, August 7, 2011, seismic event at Nafpaktos, Greece, a 3C temporary seismic station was installed in the area, to enhance the monitoring of the aftershock sequence. The station consisted of a 1-Hz LandTech LT100 sensor installed at a depth of 1 m and 24-bit LandTech LTSR-24 recorder connected to a global positioning system (GPS). The recording took place for a period of 15 days with a sampling frequency of 100 Hz. From the continuous recording, a total number of almost 150 microearthquakes, of magnitudes 0.5–1.5 M_w and shallow hypocenters up to 13 km, were detected using a chi-squared-based test statistic (Lois et al., 2010) and the P-phase arrival times were identified using the kurtosis criterion (Tselentis et al., 2011; Saragiotis et al., 2002). The detected events were verified by an expert analyst in several stations (at least three) from a permanent local network at 2 up to 12 km from the station used in the analysis. This ensured that the specific events were microearthquakes and not some other kind of energy recorded (e.g., noise bursts, anthropogenic noise, etc). Moreover, the validity of the automatic P-onsets was confirmed by the expert analyst who finally chose 110 seismic events as input data set for the proposed S-wave identification algorithm. The criterion for the selection of the specific data set was the ability of the analyst to pick most of the S-onset times, with low degree of uncertainty.

RESULTS

The proposed algorithm has been applied on the specific set of local earthquake data and the results are compared with the S-picks provided by the analyst. From the 110 manual picks, 39 picks (35.4%) were considered by the analyst as good-quality picks, 67 (60.9%) as average-quality picks, and 4 (3.7%) as poor-quality picks indicating high level of uncertainty. Moreover, the data set consisted of microearthquakes superimposed over various levels of noise, specifically from 3 dB corresponding to low S/N, up to 35 dB corresponding to high-quality signal. In Figures 4 and 5, examples of seismic events with high and low S/N are illustrated. In our experiment, we used four different windows with lengths that were empirically selected to be 0.4, 0.5, 0.6, and 0.7 seconds, respectively, according to the average S-P time difference, which was 1.1 seconds. Specifically, we selected the aforementioned lengths with respect to the half of the average S-P time difference. Moreover, the t-parameter was selected to be 0.8 seconds for q-evaluation, and also no filtering procedure took place. An example of the algorithm's performance is presented in Figure 6.

The implementation of the proposed technique resulted in an average residual time of 0.0517 seconds, corresponding to more than five samples. The term residual time refers to the mean value of the absolute difference of the manual pick to the automatic pick. Moreover, 32 picks (29.1%) were classified into uncertainty class A, 62 (56.4%) into class B, 16 picks (14.5%) into class C, and no picks were classified into class D. From the above results, it is evident that the algorithm is able to perform sufficiently well on this kind of data.

To elaborate the evaluation of the proposed technique, a noise robustness test was designed using artificial and real seismic noise. An example of the effect of this procedure for both cases is depicted in Figures 7 and 8, respectively. In the first case, Gaussian distributed noise was scaled and added to the initial data set, to achieve S/N range from 0 up to 8 dB. The algorithm's implementation on the new data set resulted in an average accuracy of 0.079 seconds, and from the new 110 automatic picks, 6 (5.5%) were classified into

class A, 63 (57.3%) into class B, 41 (37.2%) into class C, and again no picks into class D.

In the second case, real seismic noise was added to the initial data set, the S/N varied from −1 up to 8 dB, and the mean residual time was 0.092 sec. Although both tests took place on almost similar noise levels, the algorithm was affected more by the addition of real seismic noise. A possible explanation to this result is the fact that real seismic noise consists of observations that are strongly
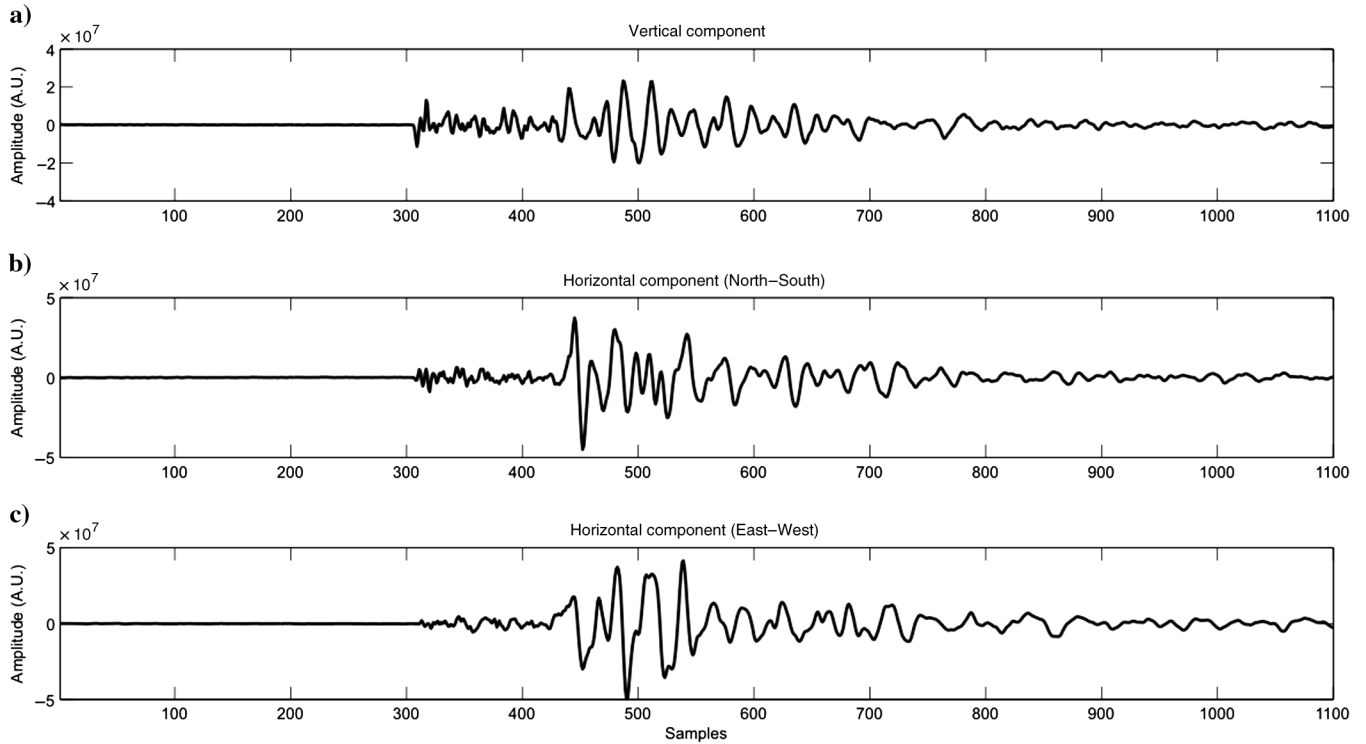

Figure 4. Example of a high-quality seismic signal.
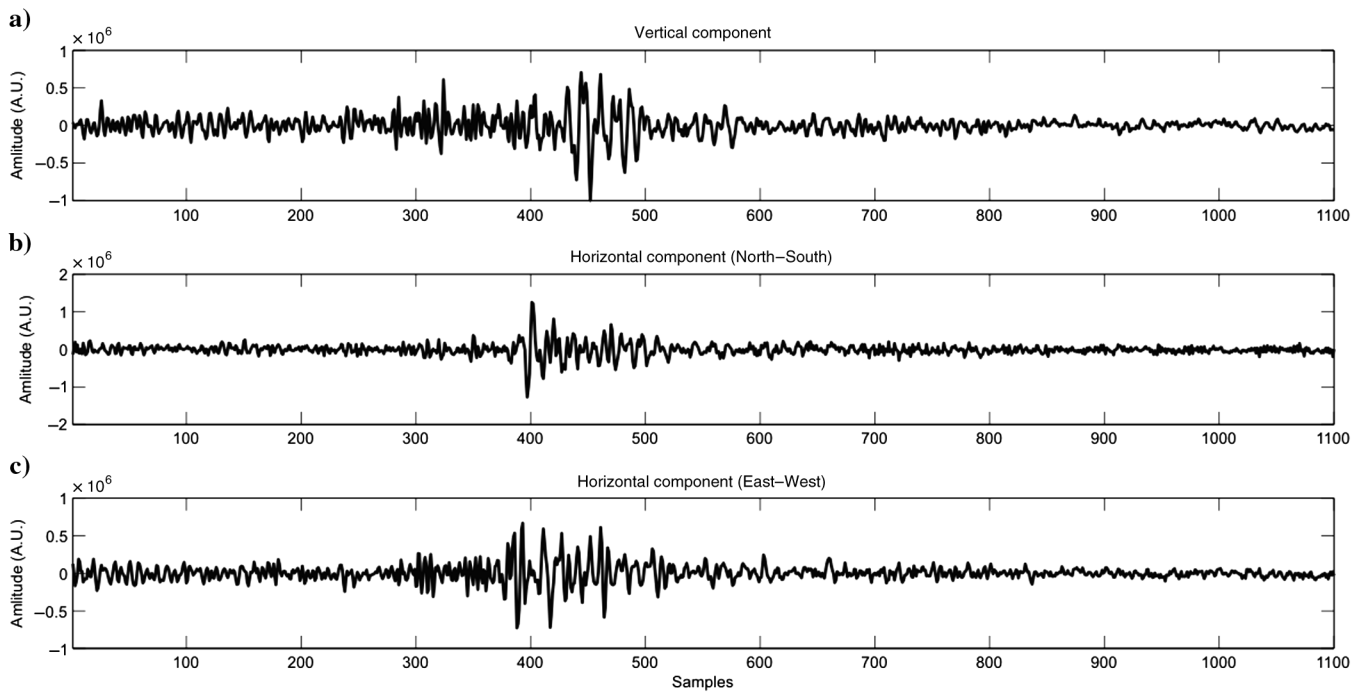
Figure 5. Example of a low-quality seismic signal.

correlated, in contrast to the synthetic Gaussian noise. The classification of the automatic picks to the uncertainty classes was the following: 5 picks (4.6%) into class A, 63 picks (57.3%) into class B, 41 picks (37.2%) into class C, and one pick (0.9%) into class D.

The distribution of the residual times as well as the picks' classification for all cases, are presented in Figure 9. However, in spite of the wide reduction of the S/N, the algorithm sustained a good performance, as long as the final mean residuals' time on both cases did
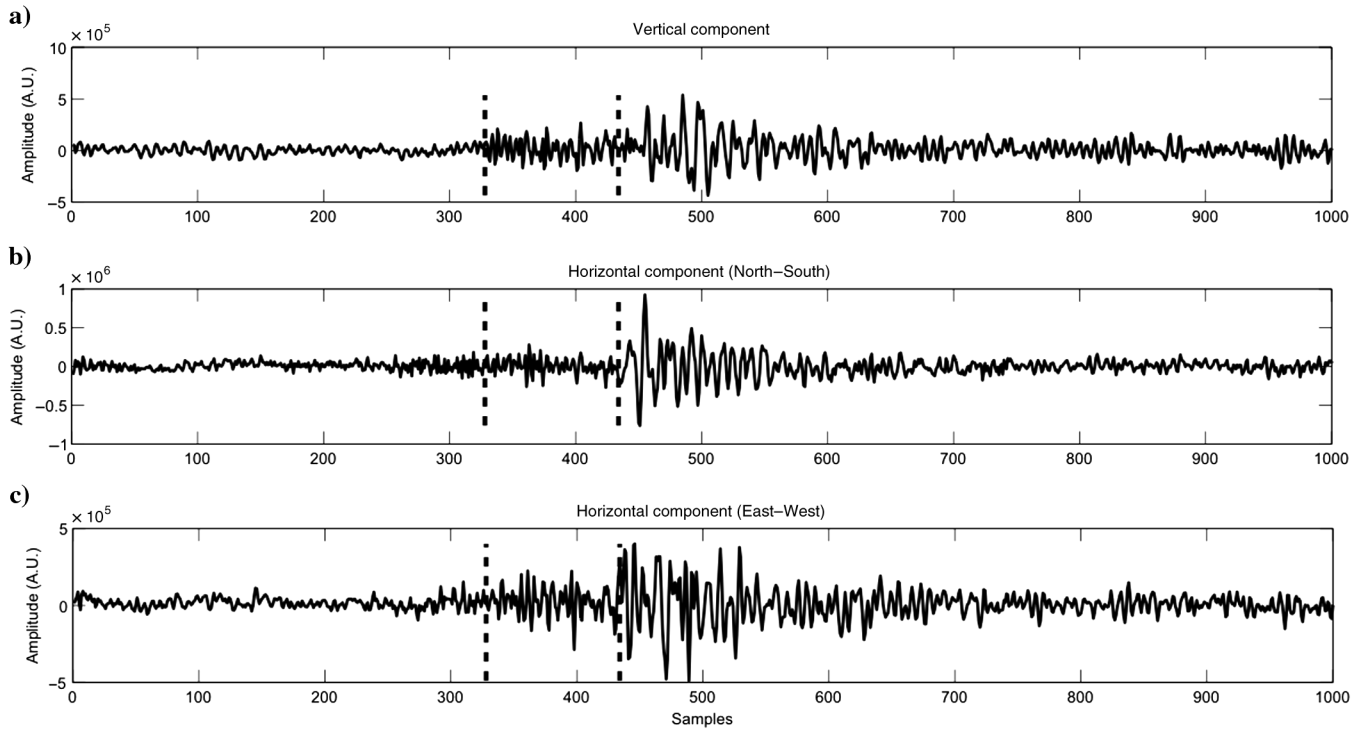
Figure 6. Example of the performance of the proposed algorithm. *P*- and *S*-arrivals are indicated by dashed lines.
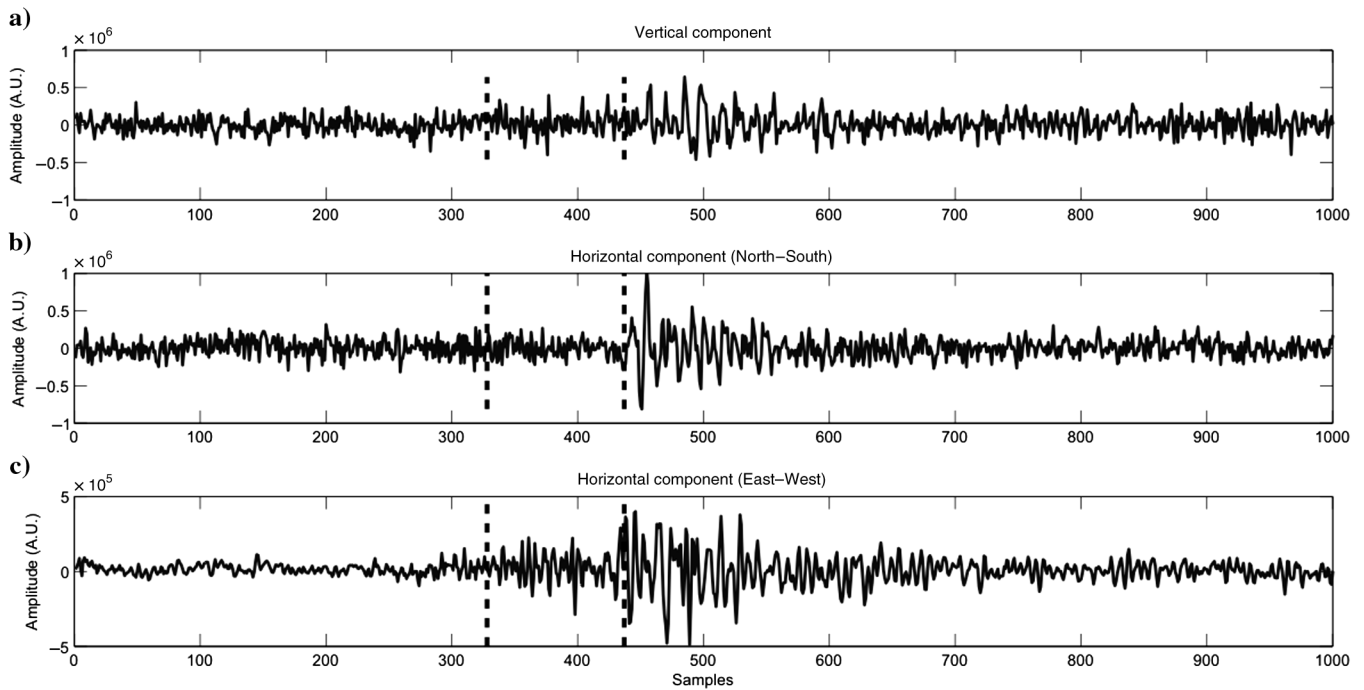
Figure 7. The effect of synthetic noise addition and the corresponding automatic *P* and *S* picks (dashed lines).
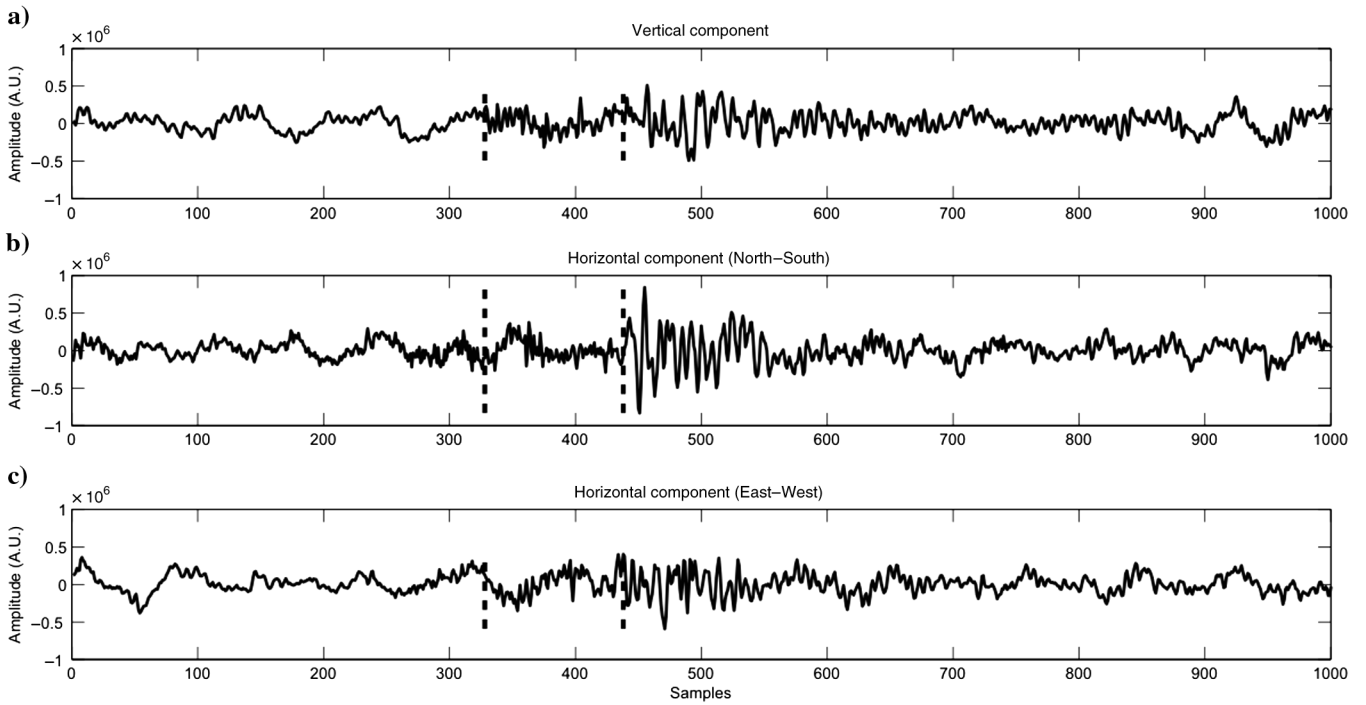
Figure 8. The effect of real seismic noise addition and the corresponding *P* and *S* picks (dashed lines).
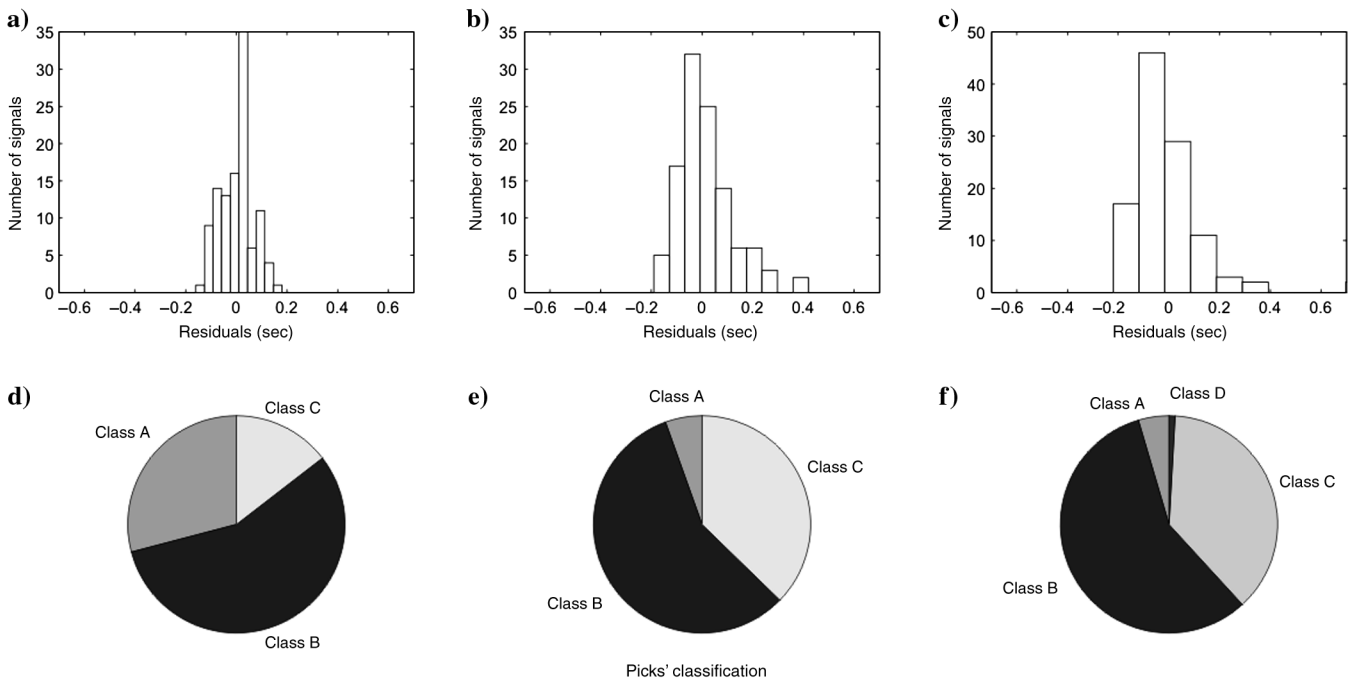

Figure 9. Histograms of the residual times and picks' classification evaluated by the algorithm. Top panel shows the histograms of the residual times for (a) the initial data set, (b) the data set resulting by the addition of Gaussian noise, and (c) the data set resulting by the addition of real seismic noise. Bottom panel (d, e, f) shows the classification of the automatic picks into the four classes, for the three aforementioned cases.

Table 1. Distribution of mean residual times for the three examined cases and each uncertainty class.

Uncertainty groups cases	Group A	Group B	Group C	Group D
Case 1: Initial data set	0.037 s	0.054 s	0.069 s	——
Case 2: Initial data set contaminated by Gaussian noise	0.053 s	0.074 s	0.09 s	——
Case 3: Initial data set contaminated by real seismic noise	0.054 s	0.082 s	0.095 s	0.8 s (outlier)

not exceed the acceptable value of 0.1 sec (10 samples). Finally, in Table 1, the mean residual time of each uncertainty group is presented for the three cases, indicating how the values of parameter q relate to the quality of automatic picks.

CONCLUSIONS

In this paper, a new approach is proposed dealing with the automatic determination of the S-wave onset time. Given the detected seismic event and the P arrival, the eigenvalue problem of data covariance matrix is solved over small time intervals. From the above analysis, a characteristic function based on the maximum eigenvalue is formed, and its statistical attributes provide a first estimation of S-onset time. Furthermore, because the algorithm's performance depends on the size of the used time window, we follow a multi-window scheme along with a weighting scenario based on energy criteria. Through this approach, a set of solutions is obtained and the weighted mean provides a final, weighted S-onset time. The algorithm's implementation on real data provided sufficiently good results in comparison with the manual picks, used as a reference data set. Moreover, the technique was subjected to a noise robustness test, using artificial and real seismic noise, resulting in an average accuracy of less than 0.1 seconds. In general, the proposed method is straightforward to implement, demands low computational resources, and the only parameters that have to be set are the lengths of the time moving windows the algorithm uses. Furthermore, earthquake location parameters are not necessary for the proposed algorithm to work properly. It is also understood that a good quality P-pick is a prerequisite to conclude on correct estimations of S-arrival time. Due to its efficiency, the specific technique can be used as a useful tool for processing seismograms obtained by microseismic networks, minimizing the necessity for human intervention.

ACKNOWLEDGMENTS

REFERENCES

Allen, R. V., 1978, Automatic earthquake recognition and timing from signal traces: Bulletin of the Seismological Society of America, **68**, 1521–32.

Anant, K. S., and F. U. Dowla, 1997, Wavelet transform methods for phase identification in three-component seismograms: Bulletin of the Seismological Society of America, **87**, 1598–612.

Baer, M., and U. Kradolfer, 1987, An automatic phase picker for local and teleseismic events: Bulletin of the Seismological Society of America, **77**, 1437–1445.

Bai, C. Y., and B. L. N. Kennett, 2000, Automatic phase-detection and identification by full use of a single three-component broadband seismogram: Bulletin of the Seismological Society of America, **90**, 187–198, doi: 10.1785/0119990070.

Chu, C.-K., and J. Mendel, 1994, First break refraction event picking using fuzzy logic systems: IEEE Transactions on Fuzzy Systems, **2**, no. 4, 255–266, doi: 10.1109/91.324805.

Cichowicz, A., 1993, An automatic S-phase picker: Bulletin of the Seismological Society of America, **83**, 180–189.

Dai, H., and C. MacBeth, 1995, Automatic picking of seismic arrivals in local earthquake data using an artificial neural networks: Geophysical Journal International, **120**, 758–774, doi: 10.1111/j.1365-246X.1995.tb01851.x.

Diehl, T., E. Kissling, S. Husen, and F. Aldersons, 2009, Consistent phase picking for regional tomography models: Application to the greater Alpine region: Geophysical Journal International, **176**, 542–554, doi: 10.1111/j.1365-246X.2008.03985.x.

Drew, J., D. Leslie, P. Armstrong, and G. Michaud, 2005, Automated microseismic event detection and location by continuous spatial mapping: Proceedings, SPE Annual Technical Conference, Paper 95513.

Duncan, P. M., and L. Eisner, 2010, Reservoir characterization using surface microseismic monitoring: Geophysics, **75**, no. 5, A139–A146, doi: 10.1190/1.3467760.

Eisner, L., T. Fischer, and T. Rutledge, 2009, Determination of S-wave slowness from a linear array of borehole receivers: Geophysical Journal International, **176**, 31–39, doi: 10.1111/j.1365-246X.2008.03939.x.

Fischer, T., A. Bouskova, L. Eisner, and J. Le Calvez, 2007, Automated P and S-wave picking of microearthquakes recorded by a vertical array, Presented at the 69th Annual International Conference and Exhibition, EAGE.

Flinn, E. A., 1965, Signal analysis using rectilinearity and direction of particle motion, Procedings of the IEEE, **53**, 1874–1876.

Gentili, S., and A. Michelini, 2006, Automatic picking of P and S phases using a neural tree: Journal of Seismology, **10**, no. 1, 39–63, doi: 10.1007/s10950-006-2296-6.

Jurkevics, A., 1988, Polarization analysis of three-component array data: Bulletin of the Seismological Society of America, **78**, 1725–1743.

Küperkoch, L., T. Meier, A. Brüstle, J. Lee, and W. Friederich and EGE-LADOS working group, 2012, Automated determination of S-phase arrival times using autoregressive prediction: Application to local and regional distances: Geophysical Journal International, **188**, 687–702, doi: 10.1111/j.1365-246X.2011.05292.x.

Lois, A., E. Z. Psarakis, V. Pikoulis, E. Sokos, and G.-A. Tselentis, 2010, A new chi-squared based test statistic for the detection of seismic events and HOS based pickers' evaluation, book of abstracts: 32nd ESC General Assembly, 129.

Magotra, N., N. Ahmed, and E. Chael, 1987, Seismic event detection and source location: Bulletin of the Seismological Society of America, **77**, 958–71.

Maxwell, S., J. Rutledge, R. Jones, and M. Fehler, 2010, Petroleum reservoir characterization using downhole microseismic monitoring: Geophysics, **75**, no. 5, A129–A137, doi: 10.1190/1.3477966.

Montalbetti, J. F., and E. R. Kanasewich, 1970, Enhancement of teleseismic body phases with a polarization filter: Geophysical Journal of the Royal Astronomical Society, **21**, 119–129, doi: 10.1111/j.1365-246X.1970.tb01771.x.

Nikias, Ch. L., and A. M. Petropulu, 1993, Higher-order spectra analysis: A nonlinear signal processing framework: PTR Prentice-Hall.

Nippress, S. E. J., A. Rietrbock, and A. E. Heath, 2010, Optimized automatic pickers: Application to ANCORP data set: Geophysical Journal International, **181**, 911–925, doi: 10.1111/j.1365-246X.2010.04531.x.

Ruud, B. O., and E. S. Husebye, 1992, A new three-component detector and automatic single station bulletin production: Bulletin of the Seismological Society of America, **82**, 221–237.

Saragiotis, C., L. Hadjileontiadis, and S. Panas, 1999, A higher-order statistics-based phase identification of three-component seismograms in a redundant wavelet transform domain: IEEE Workshop on Higher Order Statistics Proceedings, 396–399.

Saragiotis, C. D., L. J. Hadjileontiadis, and S. M. Panas, 2002, PAI-S/K: A robust automatic seismic *P* phase arrival identification scheme: IEEE Transactions on Geoscience and Remote Sensing, **40**, 1395–1404, doi: 10.1109/TGRS.2002.800438.

Sokos, E., J. Zahradnik, A. Kiratzi, J. Jansky, F. Gallovic, O. Novotny, J. Kostelecky, A. Serpetsidaki, and G. A. Tselentis, 2012, The January 2010 Efpalio earthquake sequence in the western Corinth Gulf (Greece): Tectonophysics, **530-531**, 299–309, doi: 10.1016/j.tecto.2012.01.005.

Tselentis, G-A., N. Martakis, P. Paraskevopoulos, and A. Lois, 2011b, High resolution passive seismic tomography (PST) for 3D velocity, Poisson's ratio ν, and P-wave quality Q_P in the Delvina hydrocarbon field, southern Albania: Geophysics, **76**, no. 3, B1–B24, doi: 10.1190/1.3560016.

Tselentis, G-A., N. Martakis, P. Paraskevopoulos, A. Lois, and E. Sokos, 2011a, A method for microseismic event detection and P-phase picking: 81st Annual International Meeting, SEG, Expanded Abstracts, 1638–1642.

Vera Rodriguez, I., D. Bonar, and M. Sacchi, 2012, Microseismic data denoising using a 3C group sparsity constrained time-frequency transform: Geophysics, **77**, no. 2, V21–V29, doi: 10.1190/geo2011-0260.1.

Vidale, J. E., 1986, Complex polarization analysis of particle motion: Bulletin of the Seismological Society of America, **76**, 1393–1405.

Wang, J., and T. Teng, 1997, Identification and picking of *S* phase using an artificial neural network: Bulletin of the Seismological Society of America, **87**, 1140–1149.